



Alloys compatibility in molten salt fluorides: Kurchatov Institute related experience

Victor Ignatiev*, Alexander Surenkov

National Research Centre, Kurchatov Institute, Moscow, Russian Federation

ARTICLE INFO

Article history:

Available online 16 May 2013

ABSTRACT

In the last several years, there has been an increased interest in the use of high-temperature molten salt fluorides in nuclear power systems. For all molten salt reactor designs, materials selection is a very important issue. This paper summarizes results, which led to selection of materials for molten salt reactors in Russia. Operating experience with corrosion thermal convection loops has demonstrated good capability of the “nickel–molybdenum alloys + fluoride salt fueled by UF_4 and $\text{PuF}_3 + \text{cover gas}$ ” system up to 750 °C. A brief description is given of the container material work in progress. Tellurium corrosion of Ni-based alloys in stressed and unloaded conditions studies was also tested in different molten salt mixtures at temperatures up to 700–750 °C, also with measurement of the redox potential. HN80MTY alloy with 1% added Al is the most resistant to tellurium intergranular cracking of Ni-base alloys under study.

© 2013 Elsevier B.V. All rights reserved.

1. Introduction

Recent years have demonstrated a growing interest in the circulating-fuel nuclear systems based on molten fluorides salts [1]. These systems present a promising flexible option in response to the goals and criteria assigned to future nuclear systems: fuel cycle sustainability, safety, environmental impact, proliferation resistance, diversity of applications and economics.

Nuclear power systems employing molten salt fluorides have been investigated by Oak Ridge National Laboratory (ORNL), USA in the 1960s and 1970s [2–4]. The favorable experience gained from the 8 MWt MSRE test reactor operated from 1965 to 1969 led to the design of a 1000 MWe molten salt breeder reactor (MSBR) with a thermal spectrum graphite moderated core, and thorium–uranium fuel cycle. 1000MWe MSBR designs of two main configurations were developed at ORNL: (1) single stream system where fissile and fertile elements are components of one molten salt mixture [3] and (2) two-fluid fuel circuit configuration where fertile and fissile materials are dissolved in separate streams [4]. In both configurations, salt(s) served as fuel and blanket fluid(s) at temperatures <700 °C. The technical feasibility of such systems, with the key parameters shown in Table 1, is now generally accepted.

The optimum fuel salt for MSBR [4] is a binary mixture of LiF and BeF₂, which have very low cross sections for absorbing neutrons (lithium is enriched to 99.995% in ⁷Li) in which fluorides of

fissile and/or fertile materials UF_4/ThF_4 are dissolved. The melt solubility of UF_4 and ThF_4 in LiF–BeF₂ is more than 20 mol% at the melting temperature of about 500 °C; the vapor pressure at 700 °C is less than 10 Pa.

MSBR [4] possesses good characteristics, but requires continuous removal of soluble fission products (removal time for lanthanides is about 30 days). Creation of such an intensive system for fission products clean up in MSBR (especially for the single stream design) is a challenge, in particular, difficulties remain with actinide losses to the waste stream and in selection of constructional materials for the fuel clean up unit.

In Russia at the Kurchatov Institute (KI), the molten salt program was started in the second half of the 1970s [5]. The experimental and theoretical studies were mainly directed at the improvement of the MSBR type concepts. From 2001 to 2007 the main focus was placed on experimental and theoretical evaluation of single stream MOlten Salt Actinide Recycler & Transmuter (MOSART) system [6,7]. It was shown that the optimum spectrum for MOSART is an intermediate/fast spectrum of a homogeneous core without a graphite moderator. A promising configuration for a 2400 MWt MOSART is a homogeneous cylindrical core with a graphite reflector filled with 100% molten 15LiF–58NaF–27BeF₂ or 73LiF–27BeF₂ salt mixture (mol%). It is feasible to design a critical homogeneous core fueled only with transuranium element (TRU) trifluorides made from UOX and MOX PWR spent fuel; the equilibrium concentration for trifluorides of actinides is truly below the solubility limit at the 600 °C minimal fuel salt temperature in the primary circuit. The maximum temperature in the fuel circuit for single stream MOSART design is well below 750 °C (see Table 1).

* Corresponding author. Tel.: +7 4991967130; fax: +7 4991966172.

E-mail address: ignatiev@vver.kiae.ru (V. Ignatiev).

Table 1

The basic characteristics of molten salt systems under consideration.

	MSBR [3,4]	MSFR [8–10]		MOSART [6,13]	
Type	Breeder	Breeder		Burner/converter	
Neutron spectrum	Thermal	Fast		Fast	
Number of fluid streams	2	1	2	1	2
Thermal capacity, MW	2250	2250	3000	2400	2400
Fuel salt temperature, °C	566/704	566/704	600/750	700/850	600/720
Fuel salt composition, in mol%	68LiF 31.8BeF ₂ 0.2UF ₄	71.8LiF 16BeF ₂ 12ThF ₄ 0.2UF ₄	77.5LiF 20ThF ₄ 2.5UF ₄	16ThF ₄ 6.5TRUF ₃	57NaF 15LiF 27BeF ₂ 1TRUF ₃
Blanket salt composition, in mol%	71LiF 2BeF ₂ 27ThF ₄	No	78LiF 22ThF ₄	78LiF 22ThF ₄	No
Fuel cycle	U-Th	U-Th	U-Th	TRU-Th-U	Without U, Th
Fission product removal time, efpd	30–50	10–30	418	418	300

Recent molten salt Th–U breeder developments in CNRS, France [8–10] also addresses advanced large power units without graphite in the core (MSFR). This has a fast neutron spectrum and the reprocessing rate is strongly reduced, down to 40 l per day, to get a positive breeding gain. For MSFR [10] the solvent system considered for fuel and blanket circuits is molten LiF–ThF₄ ($T_{\text{melting}} = 565^\circ\text{C}$). Compared to MSBR, the basic difficulty of MSFR is that it essentially requires a higher starting loadings of fissile materials (5060 kg of UF₄ or 11,200 kg of TRUF₃) and a higher fuel concentration for criticality [8,9] (see Table 1). In MSFR the starting loading [10] concentration of UF₄ (TRUF₃) in fuel salt will be 2.5 (6.5) mol%. Because of limits on solubility of TRUF₃ a molten 78LiF–16ThF₄–6.5TRUF₃ salt mixture (mol%) can be realized only if the minimum temperature in the fuel circuit is $>700^\circ\text{C}$ [11,12]. In this case the maximum temperature of fuel salt in the core is 850 °C [10]. At the same time, an MSFR with 77.5LiF–20ThF₄–2.5UF₄ starting loading can operate with a maximum temperature in the fuel circuit $<750^\circ\text{C}$ [6].

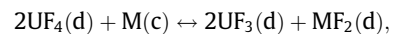
Combining the MOSART system with a Th containing molten salt blanket [13], can provide (1) core operation with minor actinide bearing fuels based on additional ²³³U support or (2) effective production of ²³³U required for starting uranium loading of MSFR. From the point of view of the reactor structure, such symbiosis of MSFR + hybrid MOSART can have an advantage, since it allows use of proven container materials at temperatures up to 700–750 °C. These observations allow us to revisit a simpler and proliferation resistant single-fluid MOSART concept. The single fluid configuration avoids also the divider metallic wall between blanket and fuel streams which in two-fluid concept has the limited lifetime not more than 5 years. The calculations [6] show the potential of Li, Be, Th/F MOSART system for operation in the self-sustainable mode with conversion ratio CR = 1 (see Table 1). The single-fluid 2400 MWt core of this type, containing as initial loading 2 mol% of ThF₄ and 1.2 mol% of TRUF₃, with the lanthanides removal cycle 300 efpd after 10 years, can operate without any TRUF₃ make up basing only on Th support as a self-sustainable system. At equilibrium the molar fraction of fertile material in the fuel salt does not exceed 5–6%.

2. Background

For all molten salt concepts mentioned above, materials selection is a very important issue. Because the products of oxidation of metals by fluoride melts are quite soluble in corroding media, passivation is precluded, and the corrosion rate depends on other factors, including: cation imbalance due to fission (also Te corrosion), atmospheric oxidants and cyclic corrosion.

Molten salt use typically begins with the acquisition of raw components that are combined to produce a mixture that has the desired properties when melted. However, most suppliers of halide salts do not provide materials that can be used directly. The major impurities that must be removed to prevent severe corrosion of the container metal are moisture and oxide contaminants. Once purified, these salts must be kept in sealed containers to eliminate atmospheric contamination in handling and storage. During the US MSR program, a considerable effort was devoted to salt purification by HF/H₂ sparging of the molten salt [13]. The experimental studies also confirmed that solid NH₄HF₂ can be efficiently used instead of HF gas for removal of oxygen-containing impurities from metal fluorides and for conversion of uranium and thorium dioxides to anhydrous tetrafluorides. In addition to removing moisture/oxide impurities, the purification also removes other halide contaminants, such as chlorides and sulfur. Methods were also developed to ensure the purity of the reagents used to purify the salts and to clean the container surfaces used for corrosion testing.

The data on standard free energies of formation for species in fuels salts [5,14] reveal that in reactions with structural metal (M):



where d and c represent solute and crystalline solid, respectively, using molten salt fluoride as reaction medium.

Chromium is much more readily attacked than iron, nickel, or molybdenum. Ni-base alloys, more specifically Hastelloy N and its later modifications, are considered the most promising for use in molten salts and have received most attention in MSR program at ORNL [14]. The chemistry of Hastelloy N was tailored to achieve compatibility with fuel salts containing UF₄ by simply allowing the melt to equilibrate with the alloy. Chemical compositions of the Hastelloy N and other Ni-base alloys later developed for MSR are given in Table 2.

A large body of literature exists on the corrosion of metal alloys by molten fluorides. Much of this work was done at ORNL and involved both thermal convection and forced convection flow loops. Tests were performed in a temperature gradient system with various fluoride media and different temperatures (maximum temperature and temperature gradient). In order to select the alloy best suited to this application, an extensive program of corrosion tests was carried out on the available commercial Ni-base alloys and austenitic stainless steels [14–21]. Chromium, which is added to most alloys for high-temperature oxidation resistance, is quite soluble in molten fluoride salts. Metallurgical examination of the surveillance specimens showed corrosion to be associated with outward diffusion of Cr through the alloy. It was concluded that the chromium content must be maintained as low as reasonably possible to retain appropriate air oxidation properties. The

Table 2

Chemical composition of the nickel-base alloys (mass%).

Element	Hastelloy-N (INOR-8)	Hastelloy-N Ti-mod.	Hastelloy-N Nb-mod.	MONICR	HN80M-VI	HN80MTY (EK-50)	HN80MT
Ni	Base	Base	Base	Base	Base	Base	Base
Cr	7.52	6–8	6–8	6.85	7.61	6.81	7.02
Mo	16.28	11–13	11–13	15.8	12.2	13.2	12.1
Ti	0.26	2	–	0.026	0.001	0.93	1.72
Fe	3.97	0.1	0.1	2.27	0.28	0.15	<0.33
Mn	0.52	0.15–0.25	0.15–0.25	0.037	0.22	0.013	<0.1
Nb	–	0–2	1–2	<0.01	1.48	0.01	–
Si	0.5	0.1	0.1	0.13	0.040	0.040	<0.05
Al	0.26	–	–	0.02	0.038	1.12	–
W	0.06	–	–	0.16	0.21	0.072	–
Cu	0.02	–	–	0.016	0.12	0.020	<0.01
Co	0.07	–	–	0.03	0.003	0.003	–
Ce	–	–	–	<0.003	0.003	0.003	–
Zr	–	–	–	0.075	–	–	–
B	<0.01	0.001	0.001	<0.003	0.008	0.003	<0.001
S	0.004	0.01	0.01	0.003	0.002	0.001	<0.001
P	0.007	0.01	0.01	0.003	0.002	0.002	<0.001
C	0.05	0.05	0.05	0.014	0.02	0.025	0.004

– The elements were neither added to the melt nor determined.

corrosion rate is marked by initial rapid attack associated with dissolution of Cr and is largely driven by impurities in the salt [14–17]. This is followed by a period of slower, linear corrosion behavior, which is controlled by a mass transfer mechanism dictated by thermal gradients and flow conditions. Minor impurities in the salt can enhance corrosion by several orders of magnitude, so impurities must be kept to a minimum. Dissolution can be mitigated by chemical control of the redox in salts, for example by small additions of elements such as Be, Cr or Zr metal. Corrosion increased dramatically as the temperature was increased and is coupled to elements plating out in the relatively cooler regions of the system, particularly in situations where high flow rates are involved.

The above reaction with UF_4 may have an equilibrium constant which is strongly temperature dependent; hence when the salt is forced to circulate through temperature gradient, a possible mechanism exist for mass transfer and continued attack. If Ni, Fe and Mo are assumed to form regular or ideal solid solutions with Cr, and if the circulation is rapid, the corrosion process for alloys in fluoride salts can be simply described [14]. At high flow rates, uniform concentrations of UF_3 and CrF_2 are maintained throughout the fluid circuit. Under these conditions, there exists some temperature (intermediate between the max and min temperature of the circuit – T_{bp}) at which the initial chromium concentration of the structural metal is at equilibrium with the melt. Since the equilibrium constant for the chemical reaction with chromium increases with increased temperature, the chromium concentration in the alloy surface tends to decrease at temperatures higher than T_{bp} and tends to increase at temperatures lower than T_{bp} . At some point in time, the dissolution process will be controlled by the solid state diffusion rate of chromium from the matrix to the surface of the alloy.

Hastelloy N alloy was the sole structural material used in the Li, Be, Zr, U/F MSRE and contributed significantly to the success of the experiment [2]. Less severe corrosion attack (<10 $\mu\text{m}/\text{year}$) was seen for the Hastelloy N in contact with the MSRE fuel salt at temperatures up to 704 °C for 3 years (26,000 h) than in the other alloys in the test. The most striking observation is the almost complete absence of corrosion for Hastelloy N during the 3-year exposure to MSRE coolant Li, Be/F salt.

Two main problems of Hastelloy N requiring further study were observed during the construction and operation of the MSRE. The first was that the Hastelloy N used for the MSRE was subject to a kind of “radiation hardening”, actually irradiation embrittlement, due to accumulation of helium at grain boundaries [2]. Later, it

was found that a modified alloy with fine carbide precipitates within the grains would trap the helium and avoid this migration to the grain boundaries. Nevertheless, it is still desirable to design MSRs in which the exposure of the reactor vessel wall to fast neutron radiation is limited. The second problem was the discovery of tiny cracks on the inside surface of the Hastelloy N piping of the fuel circuit. It was found that these cracks were caused by the fission product tellurium [18–20]. Later work showed that tellurium attack could be controlled by keeping the fuel on the reducing state. This is done by adjustment of the chemistry so that about 2% of the uranium is in the form of UF_3 , instead of UF_4 . This can be controlled rather easily now that good analytical methods have been developed (see below). If the UF_3 to UF_4 ratio becomes too low, it can be raised by the addition of beryllium metal, which, as it dissolves, will react with some of the fluoride ions from the UF_4 .

The significance of redox control in the MOSART system with uranium-free fuel is that in some cases, where the fuel is e.g. PuF_3 , the $\text{Pu}(\text{III})/\text{Pu}(\text{IV})$ redox couple is too oxidizing to provide a satisfactory redox buffered system. In this case, as was proposed by ORNL, redox control could be accomplished by including an HF/H_2 mixture in the inert cover gas sparge, which will not only control the redox potential, but will also serve as the redox indicator when the exit HF/H_2 stream is analyzed and compared to inlet stream composition. For 10 MWt reactor system similar to MSRE but run with PuF_3 it is calculated that as little as 1 cc/min HF would be required to compensate for the net reducing effect of plutonium fission [20].

The research toward finding a material for constructing a MSR that has adequate resistance to irradiation embrittlement and intergranular cracking (IGC) by tellurium has made progress [21,22]. The last reported ORNL findings strongly suggest that a MSR could be constructed of 1- to 2%-Nb-modified Hastelloy N and operated very satisfactorily at 650 °C.

3. Experimental

In Russia, materials testing for MSRs was started at the KI in 1976 [5]. It was based on data accumulated in the ORNL MSR program on nickel-base alloys for UF_4 -containing salts. Our MSR program included: (1) development of structural material for the MSR primary circuit based on Hastelloy-N, which is compatible with this environment and has acceptable mechanical properties, both

Table 3

Summary of Russian loop corrosion tests for molten fluoride salts [19,20].

Loop	Salt, mol%	Specimens material	T_{\max} , °C	ΔT , °C	Exposure time, h	Corrosion rate, $\mu\text{m/year}$
Solaris	46.5LiF–11.5NaF–42KF	12H18N10T HN80MT	620	20	3500	250 22
C1	92NaBF ₄ –8NaF	12H18N10T	630	100	1000	250
C2		AP-164	630	100	1000	50
C3		HN80MT	630	100	1000	12
F1	71.7LiF–16BeF ₂ –12ThF ₄ –0.3UF ₄ + Te	HN80MT	750	70	1000	3
F2		HN80MTY	750	70	1000	6
M1	66LiF–34BeF ₂ + UF ₄	12H18N10T	630	100	500	20
KURS	66LiF–34BeF ₂ + UF ₄	12H18N10T	750	250	750	25
NC-1	15LiF–58NaF–27BeF ₂ + PuF ₃	HN80M-VI HN80MTY MONICR	700	100	1600	5 5 19
Te-1	15LiF–58NaF + 27BeF ₂ + Cr ₃ Te ₄	HN80M-VI HN80MTY MONICR	700	10	400	–
Te-2	73LiF–5BeF ₂ –20ThF ₄ –2UF ₄ + Cr ₃ Te ₄	HN80M-VI HN80MTY HN80MTW	750	40	1250	–3
Te-3	71LiF–27BeF ₂ –2UF ₄ + Cr ₃ Te ₄	HN80M-VI HN80MTY HN80MTW	780	40	750	–

unirradiated and after exposure to maximum temperatures up to 800 °C; (2) tests of corrosion resistance of domestic nickel-base alloys and steels under various operation conditions and the selection of the most promising among them.

Corrosion resistance of materials was studied by two methods. The first is the method of static capsule isothermal test of reference specimens in various molten-salt mixtures; and second, tests of materials in forced and natural convection loops with thermal gradients. Not only high purity, but also high oxidation conditions were present in the loops. The latter conditions made it possible to estimate limiting corrosion characteristics of materials. A summary of loop corrosion tests for fluoride fuel and coolant salts is given in Table 3.

Special attention was given to purification of molten salt by removing impurities. In general before filling the loop for the main corrosion tests there are two procedures: (1) refill the loop with fresh pure salt and (2) and remove oxygen, nickel and iron impurities from the fresh salt. The second process also led us to the neces-

sity of salt charge purification to remove oxidants in order to reduce the redox potential to values acceptable for corrosion studies.

On the basis of available data and thermodynamic assessment of the molten salt state, the following order of operations for the salt purification was adopted [7]: (1) Hydrofluorination of salt using a mixture of hydrogen fluoride and helium to remove solid and dissolved oxides; (2) Electrolysis of the salt with the goal of removing most of the dissolved nickel and (3) Treatment of salt by metallic beryllium in order to remove the remaining nickel and iron ions. The supply vessel was equipped with additional auxiliary devices and gas lines for these purification procedures (see Fig. 1).

As can see from Fig. 2 recently built NC – type loop test facilities consist of a main system (molten salt containing units) located in a special compartment and auxiliary systems: gas–vacuum system, heat removal system, electric power supply system, system of heaters, control and measuring system of facility parameters. The

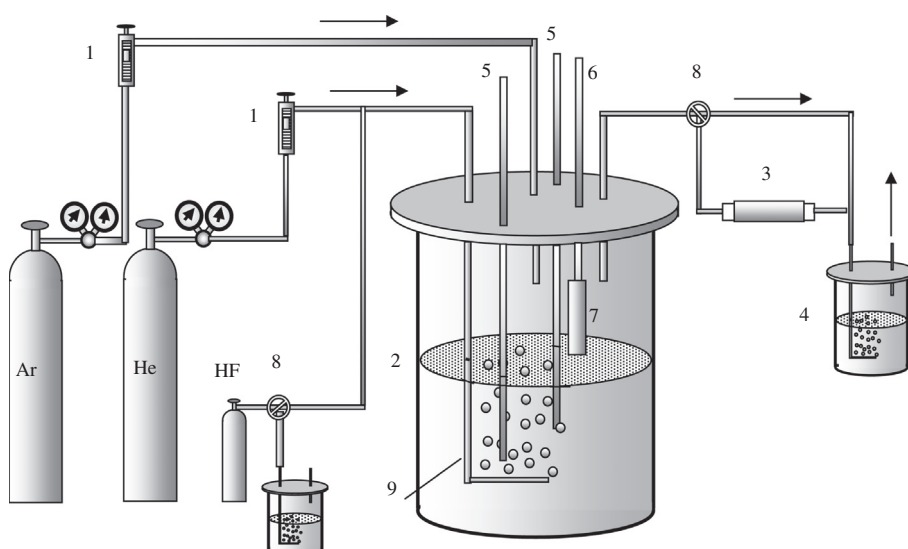
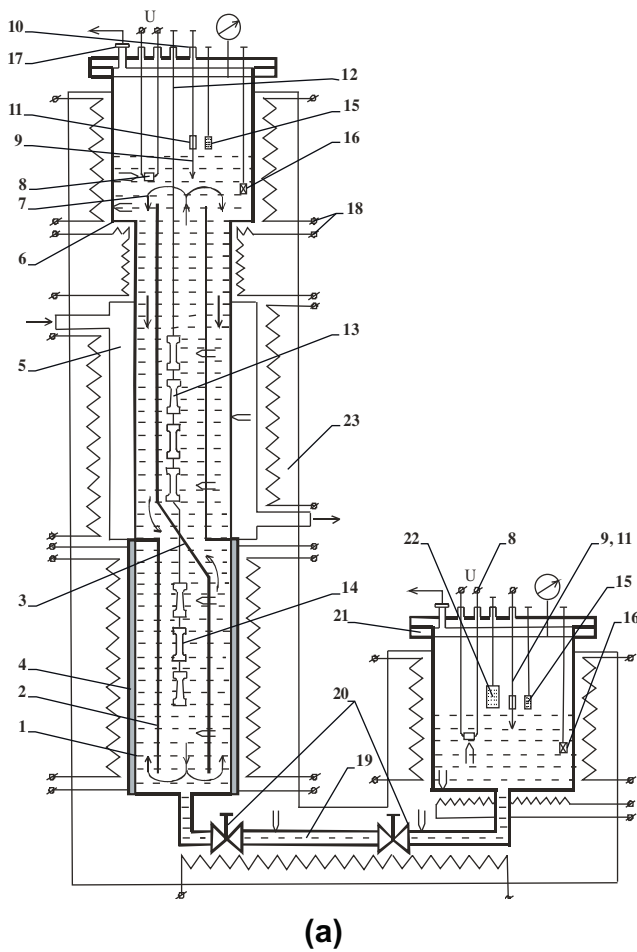
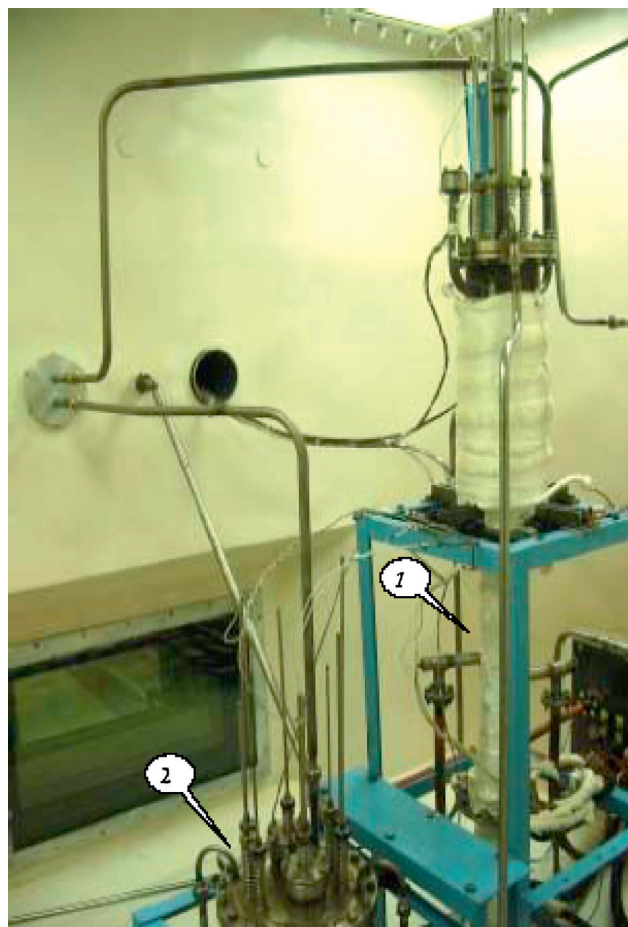


Fig. 1. Experimental set up for Li, Be, Na/F melt purification: 1 – rotameter, 2 – supply vessel/drain tank, 3 – humidity indicator, 4 – bubbler, 5 – graphite anode, 6 – gas removal line, 7 – metallic beryllium rod, 8 – valve, and 9 – isolated copper tube.



(a)



(b)

Fig. 2. Li, Be, Na, (Pu)/F corrosion loop diagram (a) and its general view in a protective isolated box (b): 1 – NP2 nickel test section of thermosyphon type; 2 – insert; 3 – inverter; 4 – main heater; 5 – forced air heat exchanger; 6 – surge tank 7 – overflowed apertures; 8 – device for the redox potential measurement; 9, 10 – level gauge; 11 – salt samplers; 12 – specimens grab; 13, 14 – material specimens; 15,16,22 – dozing devices; 17 – gas line; 18 – heaters; 19 – salt pipe; 20 – salt valve; 21 – salt supply vessel; 23 thermal insulation.

thermal NP2-grade nickel alloy convection loop of thermosyphon type connected to salt supply vessel, was equipped by heaters, thermocouples, helium/argon gas supply and associated gas purification system, and array of control/alarm system. This type of facility, the thermal convection corrosion loop with 1.2 m height, makes it possible to carry out experiments with molten salt with a temperature gradient of 80–100 °C and flow rate up to 5 cm/s ($Re \geq 3000$). Material specimens are installed both in cold and hot sections of the loop. Two salt mechanical valves at the bottom of the loop kept the molten salt from flowing back into the salt supply vessel.

Te-1, Te-2 and Te-3 facilities (see Table 3) were developed for tests of the Ni-base alloys resistance in the presence of tellurium in stressed and unstressed conditions up to 780 °C. Layout of corrosion facility is shown on Fig. 3. Corrosion facility consists of outer vessel with 300 mm diameter and 600 mm height made of stainless steel. At the top the outer vessel is sealed by a lid. Pressure down to 0.1 Pa or argon atmospheres can be maintained inside the vessel. Two heaters installed on radial and bottom surfaces of the vessel permit to maintain its temperature in lower part about 800 °C. Lower part of the outer vessel is thermally insulated. Inner salt vessel is made of nickel of NP-2 grade with 140 mm diameter and 440 mm height. The salt volume is 3 l, and its working height is 200–250 mm. To provide heating the cable heater in stainless steel shell is installed on external surface of salt vessel. Analytical

ports and instrumentation consisted of arrangements for the salt temperature measurement, removing the salt samples and material specimens from the test section plus devices for salt level. Two cassettes with the 14 specimens were submerged into the melt in such a way that four upper specimens were in the gas phase and the others – in the liquid phase. These specimens were under the permanent action of a tensile load, creating the stress in their test region. Four cassettes with 24 specimens of the same alloys were exposed to the salt mixture under similar conditions, but without any mechanical stress. The plate with chromium telluride (Cr_3Te_4) pellets was dipped onto the melt pool bottom, and it was periodically set in motion, in such a way providing the melt's forced mixing and tellurium flow to all of the specimens.

The facilities described above include the systems for redox potential measurement during corrosion studies [7,24]. A diaphragm-free three-electrode meter with a nonstationary (dynamic) beryllium reference electrode was used to measure the redox potential of the BeF_2 and PuF_3 containing salts in the corrosion loops NC 1 and Te 1 [7,25]. In its operation the electrode relies on deposition of a short-lived beryllium coating on the molybdenum cathode half-immersed into the melt in a three-electrode electrochemical cell. For this purpose, a DC pulse is passed between the cathode and the glassy-carbon anode. After the polarization current is cut off, the time variation of the emf is measured between the prepared dynamic beryllium electrode and the molybdenum indicator

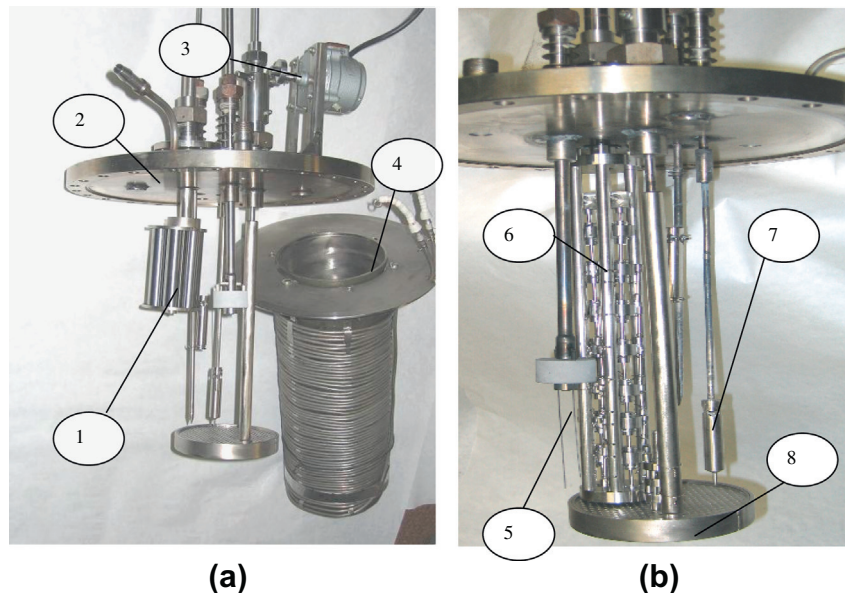


Fig. 3. Layout of Te corrosion test section: (a) test section beryllium metal reducer – 1, lid – 2, electromechanical mixer – 3, salt vessel with heater – 4; (b) device for measuring of redox potential – 5, cassettes of alloy specimens – 6, sampler/level meter – 7, plate with granulated chromium telluride – 8.

electrode, which is irreversible relative to the melt ions and has a potential equal to the redox potential of the medium. The cathode of the 3-electrode cell is polarized in the galvanostatic regime and the change of the cathode potential (with the current applied and cut off) relative to the nonpolarized indicator electrode is observed. The reference electrode potential is assumed to be zero in processing of the experimental data. Consequently, in the first horizontal section of the curve the emf of the open-circuit cell is numerically equal to the redox potential of the test melt, which is measured relative to the beryllium reference electrode, but has the opposite sign.

Results of corrosion experiments in the corrosion loops NC 1 and Te 1 demonstrated reliability of this design for measuring the redox potential in 15LiF–58NaF–27BeF₂ salt mixture containing plutonium and tellurium (see Figs. 4 and 5). It was shown that the three-electrode meter with a dynamic reference electrode is highly sensitive to changes in the redox potential of the melt and measures these changes to within ± 5 mV. As can be seen from Fig. 4, changes in measured redox potential were observed after 200 h and 850 h from the NC 1 corrosion loop start up. Both peaks on the curve result from alloy specimen removal and subsequent

ingress of laboratory atmosphere into the loop. After these jumps, redox potential decreased within 50–100 h down to the values that are slightly higher than initial ones. Average value of redox potential during corrosion test was in the range 1.25–1.33 V, corresponding to low oxidizing state of salt. This fact also confirms the analysis of salt samples. The redox potential change measured relative to dynamic Be reference electrode in Te corrosion test section vs. specimen's exposure time is shown in Fig. 5. As can see after 30 h exposure of the alloys the first sample of the melt was taken at measured redox potential $E = 1.08$ V. It corresponds to strong reduction conditions of the melt. That conclusion is in agreement with the low concentrations of oxidizers in the molten salt mixture. Slight increase in the redox potential up to $E = 1.20$ V took place in the first 100 h of the exposure. To the end of the tests its value stabilized at the level of $E = 1.18$ V.

Recent studies [26] with molten LiF–ThF₄ mixtures containing up to 2.5 mol% of UF₄ have showed that reproducible and analyzable cathodic and cyclic voltammograms can be measured only in partially reduced melts with UF₃ additions, which are free from electropositive impurity ions. Linearity of the dependence i_{pc} vs. $[UF_4]$ and i_{pc} vs. $V_{1/2}$, as well as the independence of the E_{pc} of v

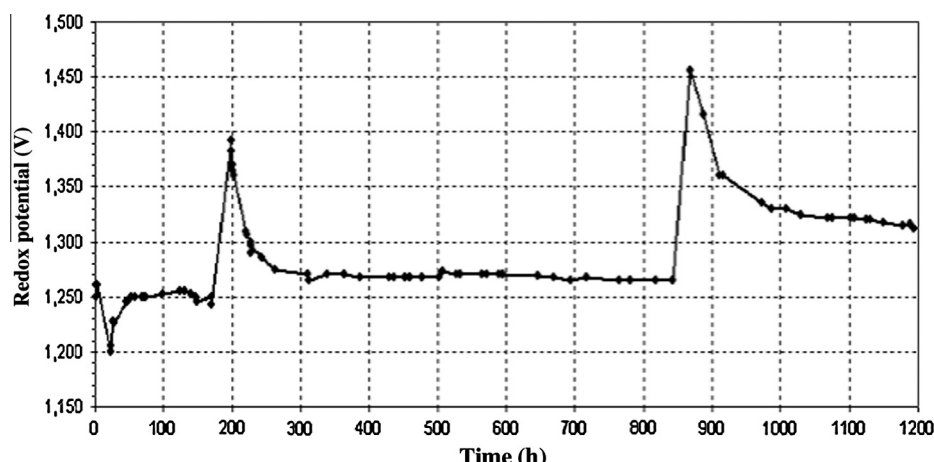


Fig. 4. Behavior of the molten salt redox potential measured relative to dynamic Be reference electrode vs. specimen's exposure time in Li, Na, Be/F corrosion loop.

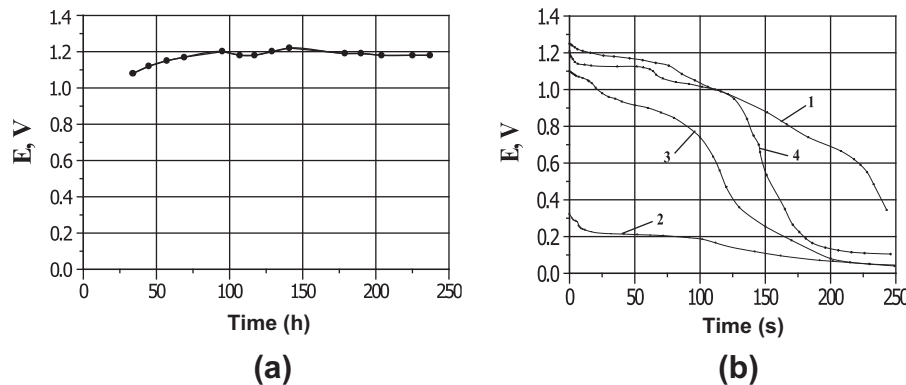


Fig. 5. Redox potential measured relative to dynamic Be reference electrode in Te corrosion test section vs. specimen's exposure time (a) and electrochemical EMF relaxation curves obtained in test section (b): after Li, Be, Na/F melt preparation (1); after melt treatment with metallic Be (2); after tellurium addition to the melt at the test start up (3) and at the end of corrosion test (4).

in the experiment are qualitatively consistent with the voltammetric criteria of reversibility of the electrode process. Platinum, tungsten or molybdenum can be used as the material of the reference and working electrodes. If the electrodes are made of different materials, the thermal emf affects the results of potentiometric and voltammetric measurements.

4. Results

In 1976 the Ni-base alloy HN80MT was chosen as a base in KI corrosion studies [5]. The composition of alloy HN80MT is given in Table 2. The development and optimization of the HN80MT alloy was mainly planned in two directions: (1) improvement of alloy resistance to selective chromium corrosion and (2) increase in alloy resistance to tellurium intergranular corrosion and cracking.

About 70 different modified alloy specimens of HN80MT were tested. Among the alloying elements varied were W, Nb, Re, V, Al, Mn and Cu. The main finding was that alloying by aluminum with a decrease of titanium by 0.5 mass% produced significant improvement of both the corrosion and mechanical properties of the alloy. Chromium corrosion and intergranular corrosion reached minimum values for an Al content of ~2.5 mass%. Irradiation effects on corrosion activity of fuels was also studied. It was shown

that at least up to a power density of 10 W/cm^3 in a molten $\text{LiF}-\text{BeF}_2-\text{ThF}_4-\text{UF}_4$ salt mixture (mol%), there was no radiation induced corrosion [5].

A subsequent radiation study of 13 alloy modifications was conducted. Specimens (in a nitrogen atmosphere) were exposed to the reactor neutron field up to a fluence of $3 \times 10^{20} \text{ n/cm}^2$. Mechanical properties of alloys were studied at temperatures of 20, 400 and 650°C for nonirradiated and irradiated specimens. The best postirradiation properties were shown for alloys modified by Ti, Al and V additions.

Corrosion of stressed material was also studied. It is known that tensile strain promotes the opening of intergranular boundaries, and thus boosts intergranular corrosion (IGC) and creates prerequisite conditions for IGC. The studies did not reveal any dependence of IGC on the stress, up to a value 240 MPa, which is 0.8 of the tensile yield of the material and 5 times the typical stresses in Li, Be, Th, U/F MSR designs.

The results of combined investigation of mechanical, corrosion and radiation properties of various alloys of HN80MT permitted the KI to suggest the Ti- and Al-modified alloy as an optimum container material for the MSR design. This alloy, named HN80MTY (or EK-50), has the composition given in Table 2.

In the thermal convection loop F2 operated with the molten $71.7\text{LiF}-16\text{BeF}_2-12\text{ThF}_4-0.3\text{UF}_4$ salt mixture (mol%) containing

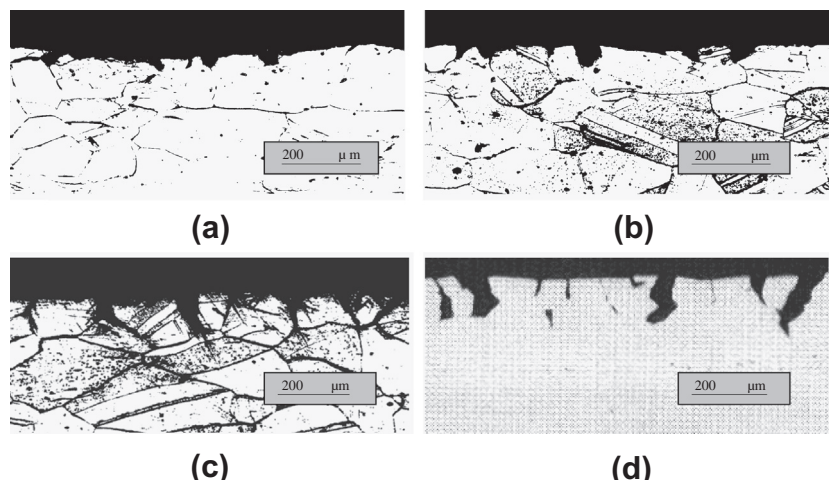


Fig. 6. Microphotographs of the Ni–Mo alloy specimens surface layer after 500 h exposure in melt $71.7\text{LiF}-16\text{BeF}_2-12\text{ThF}_4-0.3\text{UF}_4$ (mol%) containing tellurium: a – HN80MT, isothermal test, $T_{\text{exposure}} = 600^\circ\text{C}$; b – HN80MT, isothermal test, $T_{\text{exposure}} = 750^\circ\text{C}$; c – HN80MT, nonisothermal loop test, $T_{\text{exposure}} = 750^\circ\text{C}$; d – standard Hastelloy-N, isothermal test $T_{\text{exposure}} = 700^\circ\text{C}$ [20].

tellurium, the HN80MTY alloy specimens have shown a maximum corrosion rate of 6 $\mu\text{m}/\text{year}$ (see Table 3), but for the HN80MT alloy from loop F1 the corrosion rate was half that value [5]. Before exposure, the salt contained: Ni – 0.04; Fe – 0.02; Cr – 0.001 (in mass%). The corrosion was accompanied by selective leaching of chromium into the molten salt, which is evidenced by the 10-fold increase in Cr concentration after a 500 h exposure [27].

The micrographs of surface layer of HN80MT and HN80MTY alloy specimens after corrosion tests in molten 71.7LiF–16BeF₂–12ThF₄–0.3UF₄ salt mixture (mol%) containing tellurium are given on Figs. 6 and 7, respectively. As can see from Fig. 6a and b under static conditions at $T = 600^\circ\text{C}$, there is only a slight tendency of HN80MT to IGC, and corrosion defects are observed along grain boundaries at a depth of 20–30 μm . With an increase of temperature to 750 °C, the defect depth increases to 60 μm . Transition to

loop tests at $T = 750^\circ\text{C}$ show even more evidence of IGC (see Fig. 6c). Massive defects in the material along the grain boundaries at full depth and further cracking over boundaries of the following grains were found. The defect depth reaches 130 μm . The alloy resistance to IGC was estimated from a parameter "K", which is the value equal to the product of the number of cracks on a 1 cm length of a longitudinal section of specimens subjected to tensile strain, multiplied by an average crack depth in μm . The estimated value for the K parameter in these conditions (capsule isothermal tests at $T = 750^\circ\text{C}$) amounts to 1300 pc $\mu\text{m}/\text{cm}$. This data sets the maximum operating temperature for HN80MT alloy in a reactor to no more than 700 °C and rigorous control of oxidation-reduction potential of the fuel salt is necessary.

A completely different picture was observed in testing HN80MTY alloy (see Fig. 7). No IGC traces were found, either in

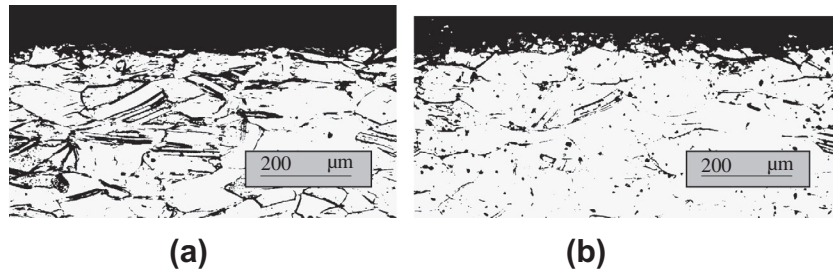


Fig. 7. Microphotographs of HN80MTY alloy specimens surface layer after 500 h exposure to the tellurium containing melt 71.7LiF–16BeF₂–12ThF₄–0.3UF₄ (mol%): a – isothermal test, $T = 750^\circ\text{C}$; b – nonisothermal loop test, $T = 750^\circ\text{C}$.

Table 4

Characteristics of intergranular corrosion for different Ni–Mo alloys after 240 h exposure in 58NaF–15LiF–27BeF₂ melt (mol%) containing chromium telluride without and with 80 MPa stress at 700 °C in test loop Te-1.

Alloy specimens	Stress	Number of cracks per 1 cm length	Average depth of cracks, μm	Maximum depth of cracks, μm	K, pc $\mu\text{m}/\text{cm}$
HN80M-VI	No	16	43	75	690
	Yes	24	65	125	1560
HN80MTY	No	14	27	37	380
	Yes	21	42	75	880
MONICR	No	115	31	44	3590
MONICR ^a	Yes			220	>10,000
Ni–7Cr–12Mo–0.5Ti–1.0Nb	Yes	23	164	220	3770
Ni–7Cr–12Mo–0.5Ti–1.0Nb–1.0Re	Yes	14	80	175	1120
Ni–7Cr–12Mo–0.5Ti–1.0Nb–0.01Y	Yes	15	79	156	1190

^a – This specimen has shown brittle fracture at minimum stress and with very low relative elongation at rupture, that many of surface cracks was not opened.

Table 5

Mechanical properties of Ni–Mo alloys before and after 1200 h corrosion test in thermal convection loop NC-1.

Alloy	Specimens conditions	Temperature, °C	σ_{02} , MPa	σ_B , MPa	δ , %
HN80M-VI	Before test (hot deformed)		1110	1210	10
	After test	605–645	870	1025	21
		650–700	725	970	35
	Before tests (quenched in water after thermo-mechanical treatment and 2 h annealing at 1100 °C)	470	800	47	
	After test	605–645	400	780	50
		650–700	370	800	50
HN80MTY	Before test (quenched in water after 1 h annealing at 1100 °C)		450	800	46
	After test	605–645	400	820	47
		650–700	410	815	53
MONICR	Before test (conditions of delivery)		510	760	52
	After test	605–645	515	763	50
		650–700	514	759	53
	Before test (quenched in water after thermo-mechanical treatment and 2 h annealing at 1100 °C)	540	890	35	
	After tests	605–645	545	898	33
		650–700	602	895	36

σ_{02} – Yield stress at 0.02% plastic strain; σ_B – ultimate tensile stress; δ – total elongation.

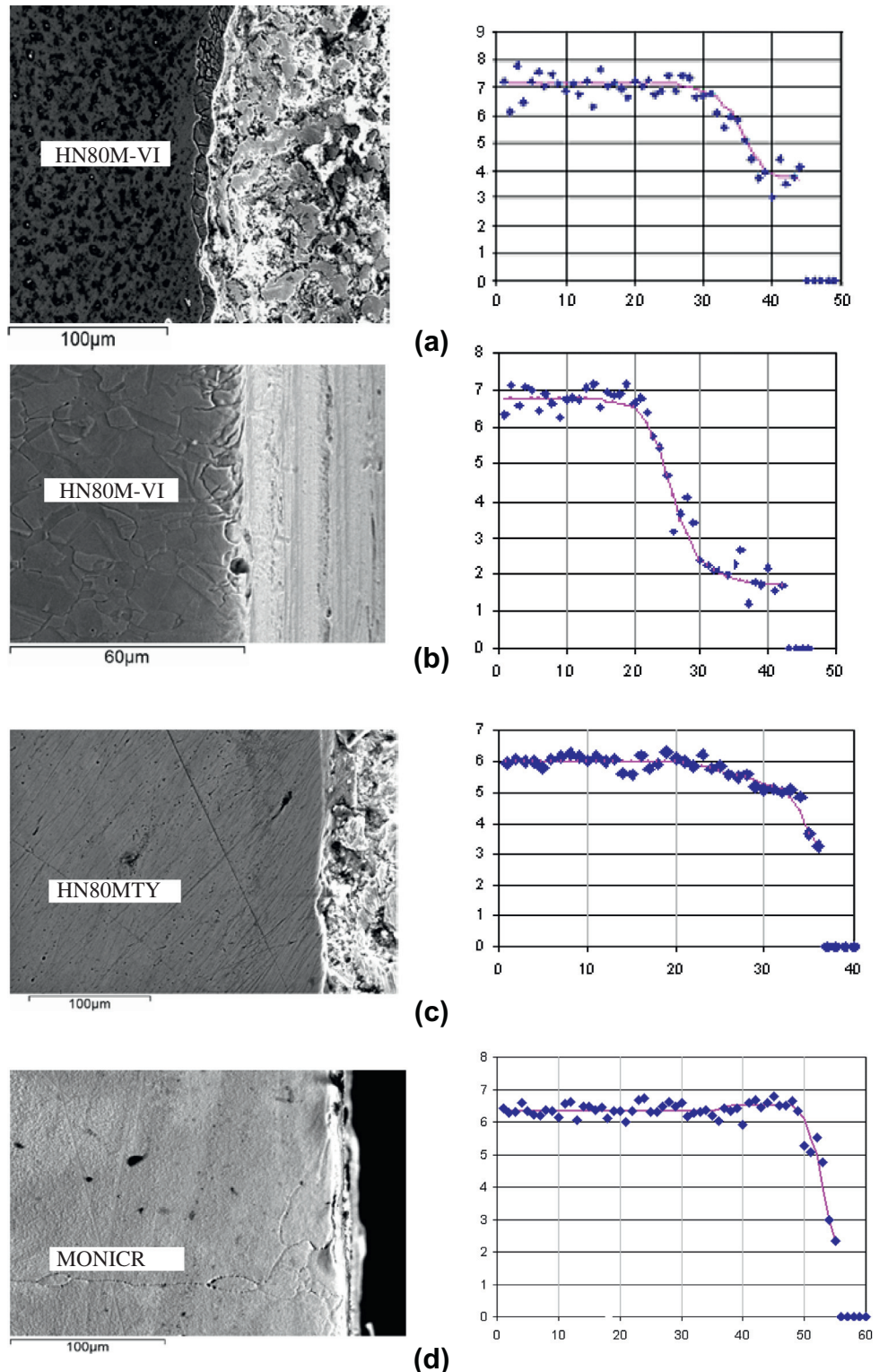


Fig. 8. Chromium distribution (mass%) vs. depth of the specimens surface layer (μm) after 1200 h exposure in corrosion loop with $15\text{LiF}-58\text{NaF}-27\text{BeF}_2$ melt (mol%) at 1.2 V redox potential: a – quenched HN80M-VI, $T = 690^\circ\text{C}$; b – hot deformed HN80M-VI, $T = 670^\circ\text{C}$; c – quenched HN80MTY, $T = 620^\circ\text{C}$; d – MONICR, $T = 690^\circ\text{C}$.

static tests under stress (at $650\text{--}800^\circ\text{C}$ with stress up to 245 MPa) or in thermal convection loops up to $T = 750^\circ\text{C}$ [27]. The thermal convection tests show that corrosion proceeds uniformly along the entire grain volume, producing a small porous layer near the surface in contact with the fuel salt, extending to a depth of 15–30 μm (see Fig. 7a and b). Thus, effective alloy modification can

solve the problem of IGC of nickel alloys in fuel salts containing fission products.

Optical microstructure studies and structural phase analysis together with data on corrosion and mechanical characteristics have shown that main reason for IGC is inhomogeneity in the solid solution, which leads to precipitation of carbide and intermetallic

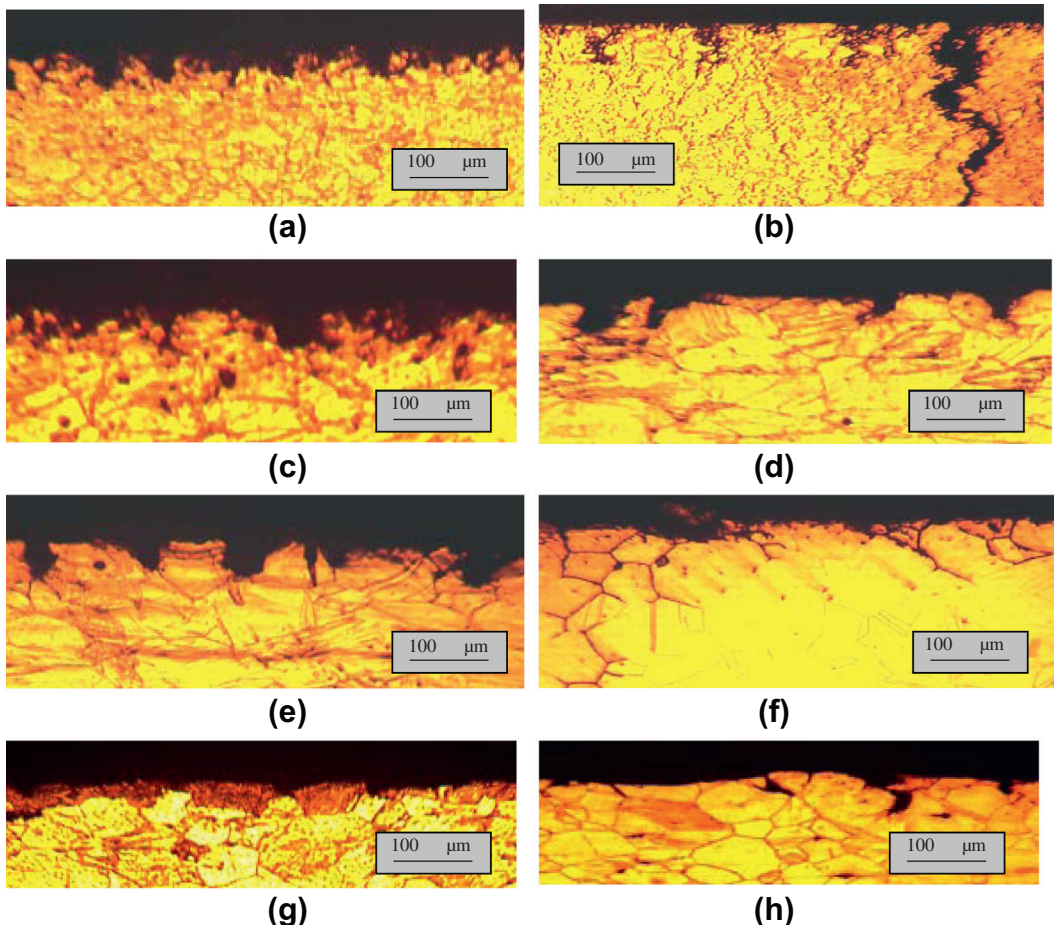


Fig. 9. Microphotographs of the Ni-based alloy specimens surface layer after 240 h exposure in 15LiF–58NaF–27BeF₂ melt (mol%) with addition of chromium telluride at 700 °C and 1.2 V redox potential without and under 80 MPa stress: (a and b) MONICR; (c and d) HN80M-VI; (e and f) HN80M 1.0% Nb; (g and h) HN80MTY 1.1%Al.

phases in the matrix and, especially on the grain boundaries. The positive effect of aluminum on resistance to Te IGC may deal with decrease and change of character of excess carbide phase on the grain boundaries: the carbide phase becomes discontinuous as round, well separated particles. Decrease of inhomogeneity also explains the increase in the corrosion resistance for HN80MTY alloy at high temperatures [5,27]. According to structural phase analysis at these conditions the process of dissolution in alloy of excess carbide phases and, especially intermetallic Ni (Al, Ti) was found. Also, alloying by aluminum increases the high-temperature strength of alloy and in some part can replace chromium in the alloy.

In a recent ISTC#1606 corrosion study the central focus was on the compatibility of Ni-base alloys with a molten Li, Na, Be/F salt mixture fueled with PuF₃ [7,24]. These studies (see Tables 3 and 4) included: (1) compatibility tests between Ni–Mo alloys and molten 15LiF–58NaF–27BeF₂ (mol%) salt in a natural convection loop with measurement of the redox potential; (2) the effect of PuF₃ addition in molten 15LiF–58NaF–27BeF₂ (mol%) salt on compatibility with Ni–Mo alloys and (3) corrosion of Ni–Mo alloys in stressed and stress-free conditions in molten 15LiF–58NaF–27BeF₂ (mol%) salt with Te added, with measurement of the redox potential. Three Hastelloy N-type modified alloys, HN80M-VI with 1.5% Nb, HN80MTY with 1% Al and MONICR [23] with about 2% Fe, were chosen for the corrosion facility study (see Table 2). Mechanical properties of Ni–Mo alloys under study are given in Table 5.

Results of a 1200-h loop corrosion experiment [24] with on-line redox potential measurement demonstrated that high temperature

operation with molten 15LiF–58NaF–27BeF₂ (mol%) salt is feasible using carefully purified molten salts and loop internals. In the established interval of salt redox potential (see Fig. 4), 1.25–1.33 V relative to a Be reference electrode, corrosion is characterized by a low rate of uniform loss of weight from sample surfaces. After this exposure the salt contained less than: Ni – 0.004; Fe – 0.002; Cr – 0.002, (in mass%). Specimens of HN80M-VI and HN80MTY alloys from the hot leg of the loop exposed at temperatures from 620 to 695 °C showed a uniform corrosion rate of 2–5 μm/year. For the MONICR alloy this value was up to 20 μm/year (see Table 3).

No significant change in corrosion behavior was found in the melt when 0.5 mol% PuF₃ was added to the 15LiF–58NaF–27BeF₂ (mol%) salt. Specimens of HN80M-VI from the loop exposed during 400 h at 650 °C showed a uniform corrosion rate of about 6 μm/year. Under such exposure, the salt contained: Ni – 0.008; Fe – 0.002; Cr – 0.002 (in mass%). No traces of IGC were found in any specimens after tests in the NC-1 loop at 1.2 V redox potential, even in the melt with the PuF₃ addition. Data from chemical analysis of the specimen's surface layer showed a decrease in chromium content to a depth of 10 to 20 μm (see Fig. 8).

Tellurium intergranular corrosion (IGC) testing of the Ni–Mo alloys [23,24], without and with stress of 80 MPa, in the 15LiF–58NaF–27BeF₂ (mol%) melt in static capsule and dynamic conditions at Te 1 facility with 1.2 V system redox potential was done at 700 °C for exposure times of 100, 250 and 400 h (see Figs. 3 and 5). Characteristics of intergranular corrosion for different Ni–Mo alloys after 240 h exposure in 58NaF–15LiF–27BeF₂ melt

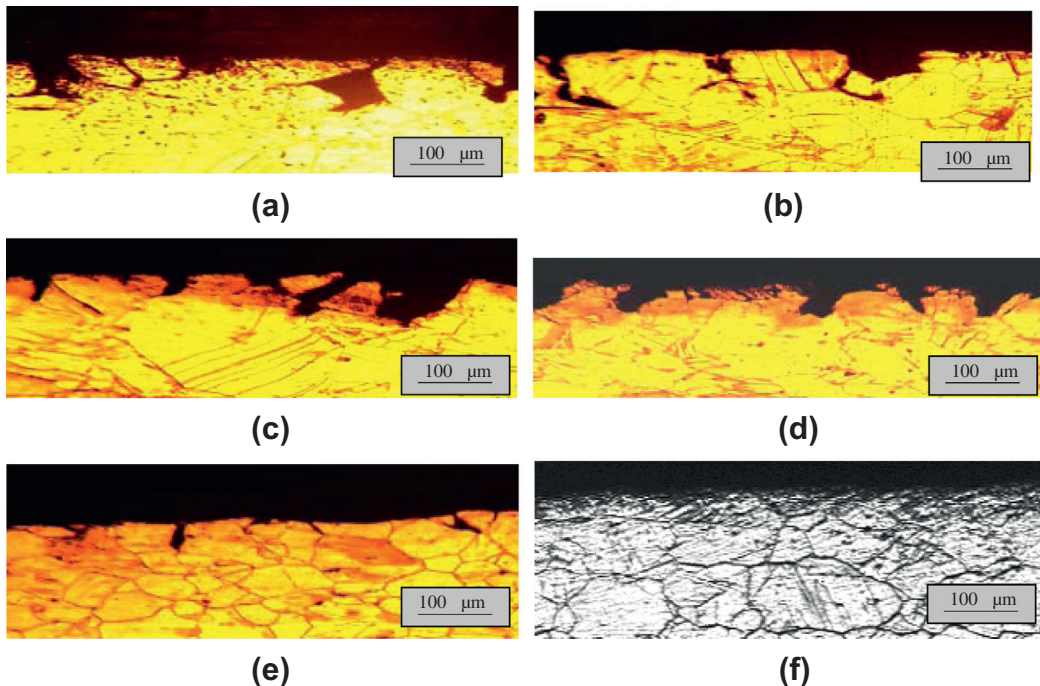


Fig. 10. Effect of Nb, Ti, Re, Y, W, Al and Mn addition to the HN80M alloy on IGC after 240 h exposure in 15LiF–58NaF–27BeF₂ melt (mol%) with addition of chromium telluride at 700 °C and 1.2 V redox potential under 80 MPa stress: (a) HN80M 0.5%Ti and 1.0%Nb; (b) HN80M 0.5%Ti, 1.0%Nb and 1.0%Re, (c) HN80M 0.5%Ti, 1.0%Nb and 0.01%Y; (d) HN80M 9.4%Mo, 1.7%Ti, 5.5%W; (e) HN80MTY 1.1%Al, (f) HN80M 0.5%Ti, 1.0%Nb and 0.25%Mn (without stress).

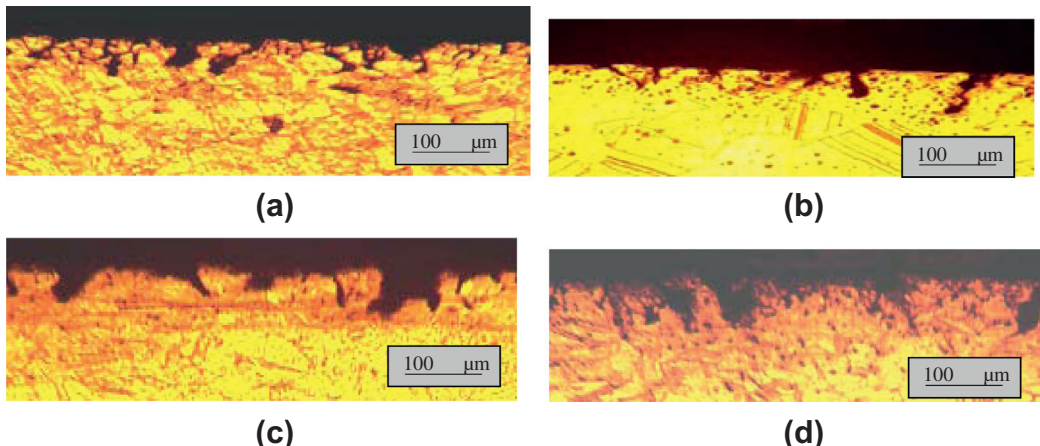


Fig. 11. Microphotographs of the HN80M alloy specimens with different Ti and Al addition after 240 h exposure in 15LiF–58NaF–27BeF₂ melt (mol%) with addition of chromium telluride at 700 °C and 1.2 V redox potential under 80 MPa stress: (a) 1.7%Ti, 0.5%Al; (b) 5.0%Cr, 1.0%Ti, 1.5%Al and without stress (c) 5.0%Cr, 0.5%Ti, 2.0%Al; (d) 5.0%Cr, 0.5%Ti, 3.0%Al.

containing chromium telluride without and under 80 MPa stress at 700 °C in test loop Te-1 are summarized in Table 4.

Microphotographs of the Ni-based alloy specimens surface layer (enlargement $\times 160$) after 240 h exposure in 15LiF–58NaF–27BeF₂ melt with addition of chromium telluride (Cr₃Te₄) at 700 °C and 1.2 V redox potential without and under 80 MPa stress: MONICR; HN80M-VI; HN80M 1.0% Nb and HN80MTY 1.1%Al are given on Fig. 9.

Fig. 9b shows that under stress exposure to tellurium in the 15LiF–58NaF–27BeF₂ melt (mol%), the depth of cracks in MONICR specimens reached 220 μm ($K > 10,000 \text{ pc} \times \mu\text{m}/\text{cm}$). For HN80M-VI specimens tested without stress, rather low IGC intensity was observed ($K = 690 \text{ pc} \times \mu\text{m}/\text{cm}$). However, under stress the intensity of the HN80M-VI alloy cracking was increased by more than a factor of two and the cracks' depth reached 125 μm

(see Fig. 9d). HN80MTY alloy is the most resistant to tellurium IGC of the Ni-Mo alloys under study (see Fig. 9h). The intensity of its cracking under stress is $K = 880 \text{ pc} \times \mu\text{m}/\text{cm}$ (half the rate of the HN80M-VI alloy).

The effectiveness on the resistance to tellurium corrosion of Nb, Al, Ti, Re and Mn doping of the HN80M-type alloy was also studied in the Li,Na,Be/F facility at the KI (see Fig. 10). It was shown that alloy doped with Nb alone significantly increases IGC resistance. As can see from Fig. 10b and c both Re and Y additions only slightly increase the alloy's resistance to tellurium cracking. Addition of W up to 5.5% in the alloy does not bring positive result (see Fig. 10d). Addition of Al or Mn gives a significant increase in alloy resistance to tellurium IGC (see Fig. 10e and f).

The maximum increase in resistance to IGC is observed for HN80M-type alloy containing 1–2 mass% of Al at decrease of Ti

down to 0.8–1 mass% (see Fig. 10e). Further decrease of the Ti down to 0.5 mass% and Cr to 5 mass%, with simultaneous increase in the Al content up to 2–3 mass% leads to strengthening of Te IGC intensity (see Fig. 11). Data of tests in molten 15LiF–58NaF–27BeF₂ salt mixture (mol%) with alloys modified by the Ti and Al confirmed that the developed HN80MTY alloy has the optimum content of Al and Ti, which gives it the maximum resistance to tellurium IGC. Results of tellurium IGC tests of Ni–Mo alloys in other fuel 73LiF–5BeF₂–20ThF₄–2UF₄ and 71LiF–27BeF₂–2UF₄ salt mixtures (mol%) at temperatures up to 750 °C will be published soon.

Therefore, testing of alloys with various compositions of doping elements to enhance the alloy resistance to tellurium IGC should be continued in a thermal convection loop with longer exposure times.

5. Conclusion

New findings in developing Ni–Mo alloys for MSRs with fuel salt temperatures up to 750 °C shift the emphasis from alloys modified with titanium and rare earths to those modified with niobium (at ORNL) and aluminum (at the KI). The next steps needed in development of these alloys must involve: (1) irradiation, corrosion, tellurium exposure, mechanical property and fabrication tests to finalize the composition for scale up; (2) procurement of large commercial heats of the reference alloy; (3) mechanical property and corrosion tests of at least 10,000 h duration; and (4) development of design methods and rules needed to design a reactor (breeder or burner) to be built of the modified alloy.

Some less mature approaches are possible and could be of interest for new MSR concepts. For example, Ni–W–Cr alloys have been recently proposed by Centre National de la Recherche Scientifique (CNRS) in France for their high potential corrosion resistance for very high temperature operation (>750 °C) [9].

Temperatures >850 °C would require the use of new solutions in selecting materials, such as refractory alloys or graphite. Further evaluation should also include assessment of (1) new proposed solvent systems, (2) increased fuel salt outlet temperatures >750 °C and (3) lower salt redox potentials from the point of view of establishing potentials that must be maintained to avoid IGC of Ni-base alloys.

Acknowledgements

This research utilized ISTC#1606 and ISTC #3749 – supported facilities at the Kurchatov Institute, VNIITF and IHTE. The authors also would like to thank Ivan Gnidoi and Vadim Uglov (Kurchatov Institute), Valery Afonichkin and Alexander Bove (IHTE) as well as Vladimir Subbotin (VNIITF) for participation in the development of corrosion facilities and materials tests.

References

- [1] C. Forsberg, C. Lebrun, E. Merlet-Lucotte, C. Renault, V. Ignatiev, Revue Generale Nucleaire 4 (2007) 63–71.
- [2] P.N. Haubenreich, J.R. Engel, Nucl. Appl. Technol. 8 (1970) 107–140.
- [3] E.S. Bettis, R.C. Robertson, Nucl. Appl. Technol. 8 (1970) 190–207.
- [4] R.C. Robertson, R.B. Briggs, O.L. Smith, E.S. Bettis, Two-fluid molten-salt breeder reactor design study, USAEC Report ORNL-4528, Oak Ridge National Laboratory, 1970.
- [5] V. Novikov, V. Ignatiev, V. Fedulov, V. Cherednikov, Molten Salt Reactors: Perspectives and Problems, Moscow, Energoatomizdat, USSR, 1990.
- [6] V. Ignatiev, O. Feynberg, A. Surenkov, V. Subbotin, V. Afonickin, M. Kormilitsyn, et al., At. Energ. 123 (2012) 127–135.
- [7] V. Ignatiev, V. Afonichkin, O. Feynberg, A. Merzlyakov, A. Surenkov, V. Subborine, et al., ISTC # 1606 Project Final Report, International Scientific and Technical Centre, Moscow, 2007.
- [8] C. Renault, S. Delpech, E. Merlet-Lucotte, R. Konings, M. Hron, V. Ignatiev, European molten salt reactor, in: Proceedings of Seventh European Commission Conference on Euroatom Research and Training in Reactor Systems, Prague, Czech Republic, 22–24 June 2009, pp. 384–399.
- [9] S. Delpech, E. Merlet-Lucotte, T. Auger, X. Doligez, D. Heuer, G. Picard, MSFR: Material Issues and Effect of Chemistry Control, in: Proceedings of GIF Symposium, Paris, France, 9–10 September 2009, pp. 201–208.
- [10] C. Renault, R. Konings, M. Hron, D. Holcomb, The molten salt reactor (MSR) in generation IV: overview and perspectives, ibid, 2009, pp. 191–200.
- [11] J.A. Fredricksen, L.O. Gilpatrick, C.J. Barton, Solubility of cerium trifluoride in molten mixtures of LiF, BeF₂ and ThF₄, USAES Report ORNL-TM-2335, Oak Ridge National Laboratory, 1969.
- [12] D. Sood, P. Iyer, R. Prasad, V. Vaidya, K.N. Roy, V. Venugopal, et al., Nucl. Technol. 27 (1975) 411–416.
- [13] J.H. Shaffer, Preparation and handling of salt mixtures for the molten salt reactor experiment, USAES Report ORNL-4616, Oak Ridge National Laboratory, 1971.
- [14] J.W. Koger, Alloy compatibility with LiF–BeF₂ salts containing ThF₄ and UF₄, USAES Report ORNL-TM-4286, Oak Ridge National Laboratory, 1972.
- [15] D.F. Williams, L.M. Toth, K.T. Clarno, Assessment of candidate molten salt coolants for the advanced high-temperature reactor, USAES Report ORNL-TM-2006/12, Oak Ridge National Laboratory, 2006.
- [16] W.D. Manly, Prog. Nucl. Energy 2 (1960) 164–179.
- [17] J.H. De Van, R.B. Evans III, Corrosion behavior of reactor materials in fluoride salt mixtures, USAEC Report ORNL/TM-328, Oak Ridge National Laboratory, 1962.
- [18] H.E. McCoy, Intergranular cracking of structural materials exposed to fuel salt, USAEC Report ORNL-4782, Oak Ridge National Laboratory, 1972, pp. 109–144.
- [19] H.E. McCoy, Intergranular cracking of structural materials exposed to fuel salt, USAEC Report ORNL-4832, Oak Ridge National Laboratory, 1972, pp. 63–76.
- [20] L.M. Toth, U. Gat, G.D. Del Gul, S. Dai, D. Williams, Review of ORNL's technology and status, in: Proceedings of Second International Conference on Accelerator Driven Technologies and Applications, Kalmar, Sweden, 3–7 June 1996, pp. 91–100.
- [21] H.E. McCoy, Status of materials development for molten salt reactors, USAEC Report ORNL-TM-5920, Oak Ridge National Laboratory, 1978.
- [22] J.R. Keiser, Status of tellurium–Hastelloy N studies in molten fluoride salts, USAEC Report ORNL-TM-6002, Oak Ridge National Laboratory, 1977.
- [23] V. Ignatiev, A. Surenkov, I. Gnidoi, V. Fedulov, V. Uglov, V. Subbotin, et al., At. Energ. 101 (2006) 278–285.
- [24] V. Ignatiev, A. Surenkov, I. Gnidoi, V. Fedulov, V. Uglov, V. Subbotin, et al., Nucl. Technol. 164 (2008) 130–142.
- [25] V. Afonichkin, A. Bovet, V. Ignatiev, V. Subbotin, A. Surenkov, A. Toropov, et al., J. Fluorine Chem. 130 (2009) 83–88.
- [26] V. Afonichkin, A. Bovet, V. Shishkin, J. Nucl. Mater. 419 (2011) 347–352.
- [27] V. Ignatiev, V. Novikov, A. Surenkov, V. Fedulov, The state of the problem on materials as applied to molten-salt reactor: problems and ways of solution, Preprint IAE-5678/11, Institute of Atomic Energy, Moscow, USSR, 1993.